

Continuum simulations of water flow past fullerene molecules

A. Popadić¹, M. Praprotnik^{1,a}, P. Koumoutsakos^{2,b}, and J.H. Walther^{2,3,c}

¹ Laboratory for Molecular Modeling, National Institute of Chemistry, Hajdrihova 19, 1001 Ljubljana, Slovenia

² Chair of Computational Science, ETH Zurich, Clausiusstrasse 33, 8092 Zurich, Switzerland

³ Department of Mechanical Engineering, Technical University of Denmark, 2800 Kgs. Lyngby, Denmark

Received 20 March 2015 / Received in final form 5 May 2015
Published online 22 June 2015

Abstract. We present continuum simulations of water flow past fullerene molecules. The governing Navier-Stokes equations are complemented with the Navier slip boundary condition with a slip length that is extracted from related molecular dynamics simulations. We find that several quantities of interest as computed by the present model are in good agreement with results from atomistic and atomistic-continuum simulations at a fraction of the cost. We simulate the flow past a single fullerene and an array of fullerenes and demonstrate that such nanoscale flows can be computed efficiently by continuum flow solvers, allowing for investigations into spatiotemporal scales inaccessible to atomistic simulations.

1 Introduction

Nanoscale flows exhibit long range hydrodynamic interactions at spatiotemporal scales that are prohibitive to molecular dynamics (MD) simulations [1]. Coarse grained and multiscale simulations can mitigate this cost at the expense of accuracy when comparing their results with those from atomistic simulations. The validity of coarse grained descriptions hinges on the choice of collective variables [2] while in hybrid models the results hinge on the information transfer between atomistic and continuum domains [3–5]. Here we present an alternative approach, where the effective description of the atomistic phenomena is reduced to one variable, namely the slip length of the water flow over a fullerene. This parameter is used to describe the critical interactions between the surface of the molecule and water and it is then provided as a boundary condition to a continuum solver.

^a e-mail: praprot@cmm.ki.si

^b e-mail: petros@ethz.ch

^c e-mail: jhw@mek.dtu.dk

Several past experiments and computer simulations suggest that the Navier-Stokes equations

$$\rho(\mathbf{v} \cdot \nabla)\mathbf{v} = -\nabla p + \mu \nabla^2 \mathbf{v}, \quad \text{and} \quad \nabla \cdot \mathbf{v} = 0, \quad (1)$$

where ρ is the fluid density, \mathbf{v} the fluid velocity, p the hydrodynamic pressure and μ the fluid viscosity, are adequate models for describing phenomena at the nanometer scale [6–12]. Bocquet and Charlaix [9] estimated the validity of the Navier-Stokes equations to confinements larger than a viscous length scale, for water it being ca. 1 nm. Experiments by Li et al. [6] showed that for hydrophobic sub-nanometer confinements water maintains its bulk viscosity. In addition, Thomas and McGaughey observed in MD simulations that the structure of water in CNTs of diameters greater than 1.4 nm is bulk-like [8]. From this we expect that the continuum description is valid when the characteristic length is larger than $\mathcal{O}(1 \text{ nm})$. A recent study also reports that in highly confined nanosize channels an extension of the Navier-Stokes equations to include the rotational degrees of freedom is needed for a correct description of fluid dynamics [13]. However, even though the Navier-Stokes equations can be suitable models for water flows at the nanoscale, experiments and simulations suggest that the well known, empirical no-slip condition is not an appropriate boundary condition to complement continuum descriptions [9, 14–20]. Instead, slippage effects have been shown to best describe the solid-liquid interface. It is important to note that in the nanoscale, with the high ratio of the interface area to the bulk volume the physics at the interface, and their corresponding boundary conditions, become increasingly important [9, 19].

2 Theoretical background

2.1 Partial slip boundary condition

In continuum descriptions of the flow field the slippage effects can be accounted for by applying the Navier boundary condition [21, 22]. The Navier boundary condition assumes a linear dependence of the fluid velocity at the wall to the wall shear stress:

$$\sigma_{ik} n_k = \lambda v_{ti} - p' n_i, \quad (2)$$

where σ_{ik} is the stress tensor, n_k the k -th Cartesian component of the normal to the wall \mathbf{n} pointing into the fluid, λ the friction coefficient between the wall and the fluid, v_{ti} the i -th Cartesian component of \mathbf{v}_t , the tangential to the wall component of fluid velocity \mathbf{v} , and p' the total pressure exerted on the wall by the fluid. Requiring the balance of the stress tensor at the wall to the stress tensor of bulk liquid [23]

$$\sigma_{ik} = \mu \left(\frac{\partial v_i}{\partial x_k} + \frac{\partial v_k}{\partial x_i} \right) - p \delta_{ik}, \quad (3)$$

where δ_{ik} is the Kronecker delta function, we obtain the velocity boundary condition

$$\lambda \mathbf{v}_t - p' \mathbf{n} = \mu [2(\mathbf{n} \cdot \nabla)\mathbf{v} + \mathbf{n} \times (\nabla \times \mathbf{v})] - p \mathbf{n}. \quad (4)$$

We further split this boundary condition into a tangential and normal components, where the normal component reads

$$p' = p - 2\mu \frac{\partial v_n}{\partial n}, \quad (5)$$

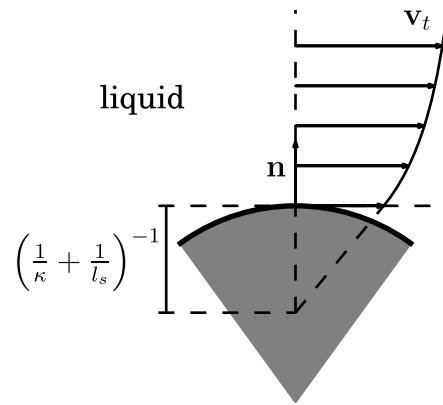


Fig. 1. Schematic of the Navier boundary condition. The shaded region represents the solid and the region above it the liquid.

where $\partial/\partial n$ represents the gradient in the direction of the normal to the wall and v_n the normal component of the fluid velocity. The tangential component on the other hand reads

$$\mathbf{v}_t = \frac{\mu}{\lambda} [2(\mathbf{n} \cdot \nabla)\mathbf{v}_t + \mathbf{n} \times (\nabla \times \mathbf{v}_t) + \mathbf{n} \times (\nabla \times \mathbf{v}_n)]. \quad (6)$$

By using the following relation

$$\nabla(\mathbf{a} \cdot \mathbf{b}) = (\mathbf{a} \cdot \nabla)\mathbf{b} + (\mathbf{b} \cdot \nabla)\mathbf{a} + \mathbf{a} \times (\nabla \times \mathbf{b}) + \mathbf{b} \times (\nabla \times \mathbf{a}) \quad (7)$$

in Eq. (6) and the Stokes theorem on the normal to the wall (\mathbf{n}) and the normal component of the velocity (\mathbf{v}_n) the boundary condition becomes

$$\mathbf{v}_t = \frac{\mu}{\lambda} [(\mathbf{n} \cdot \nabla)\mathbf{v}_t - (\mathbf{v}_t \cdot \nabla)\mathbf{n}]. \quad (8)$$

The first term on the right is the gradient of the tangential component of velocity in the direction normal to the wall and the second term is the curvature of the wall in the flow direction. The boundary condition can thus be written in a more compact form [12]

$$v_t = l_s \left[\frac{\partial v_t}{\partial n} - \frac{v_t}{\kappa} \right], \quad (9)$$

where κ is the radius of the curvature of the wall in the flow direction with the curvature being negative for concave boundaries (Fig. 1). In Eq. (9) we introduce the slip length $l_s = \mu/\lambda$, which for noncurved boundaries ($\kappa \rightarrow \infty$) gives the depth at which the linear extrapolation into the wall of the fluid velocity vanishes. The boundary condition Eq. (9) differs slightly from the more intuitive and frequently used boundary condition

$$v_t = l_s \frac{\partial v_t}{\partial n} \quad (10)$$

in the presence of an additional interface curvature dependent term. The importance of the curvature term was emphasized by Einzel et al. [24] The omission of the interface curvature dependent term would result in the dependence of slip length from interface curvature and it could also result in a negative slip length. In the case of the boundary condition in Eq. (9), however, the slip length is always positive since the slip length is defined as the ratio of viscosity and the interface friction coefficient, of which both are positive. The slip length might still, however, vary with the interface curvature as a

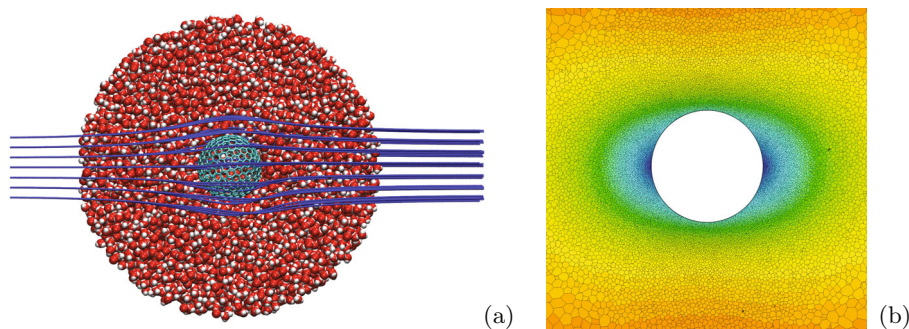


Fig. 2. Illustrations from simulations of flow past a C_{540} fullerene molecule: (a) multi-scale simulations coupling an atomistic MD description with a continuum Lattice-Boltzmann model [5]; (b) continuum Navier-Stokes model subject to the partial slip, Navier boundary condition.

consequence of the interface friction coefficient dependence on the interface curvature as is suggested by several past studies [7, 25, 26].

The slip length or the interface friction coefficient can be extracted from MD simulations [9, 21, 25–31].

2.2 Continuum hydrodynamics

In a recent study by Walther et al. [5] a multiscale simulation of water flow past a C_{540} fullerene molecule was performed by coupling MD to the Lattice-Boltzmann method cf. Fig. 2a. A steady state solver was used to describe the flow in the continuum domain and the atomistic-continuum coupling relied on the Schwarz domain decomposition algorithm. An important feature of this coupling was the transfer of gradient information between the continuum and atomistic descriptions ensuring momentum conservation. In the present work we tackle the same problem by employing a fully continuum description coupling finite volume simulations of the Navier-Stokes equations with Navier boundary conditions applied on the interface between the fullerene molecule and the fluid (Fig. 2b). Far field boundary conditions are set to mimic the boundary conditions from the multiscale simulations of Walther et al. [5].

By matching the drag force measured in continuum flow simulations to the drag force measured in the multiscale simulation we extract the slip length for the water flow past the C_{540} fullerene molecule. The non-dimensional drag force reads as

$$F^* = F \frac{1}{\rho v_\infty^2 R^2} \quad (11)$$

where F is the drag force on the fullerene molecule and F^* the drag force in the non-dimensional form. v_∞ is the upstream velocity and $R = 1.03$ nm the radius of the fullerene molecule. Hereinafter the variables denoted with a star represent non-dimensionalized variables, where length is scaled as $x^* = x/R$, velocity as $v^* = v/v_\infty$.

3 Results

We perform our simulations using the STAR-CD simulation package into which we have implemented the Navier boundary condition [32]. We perform two sets of

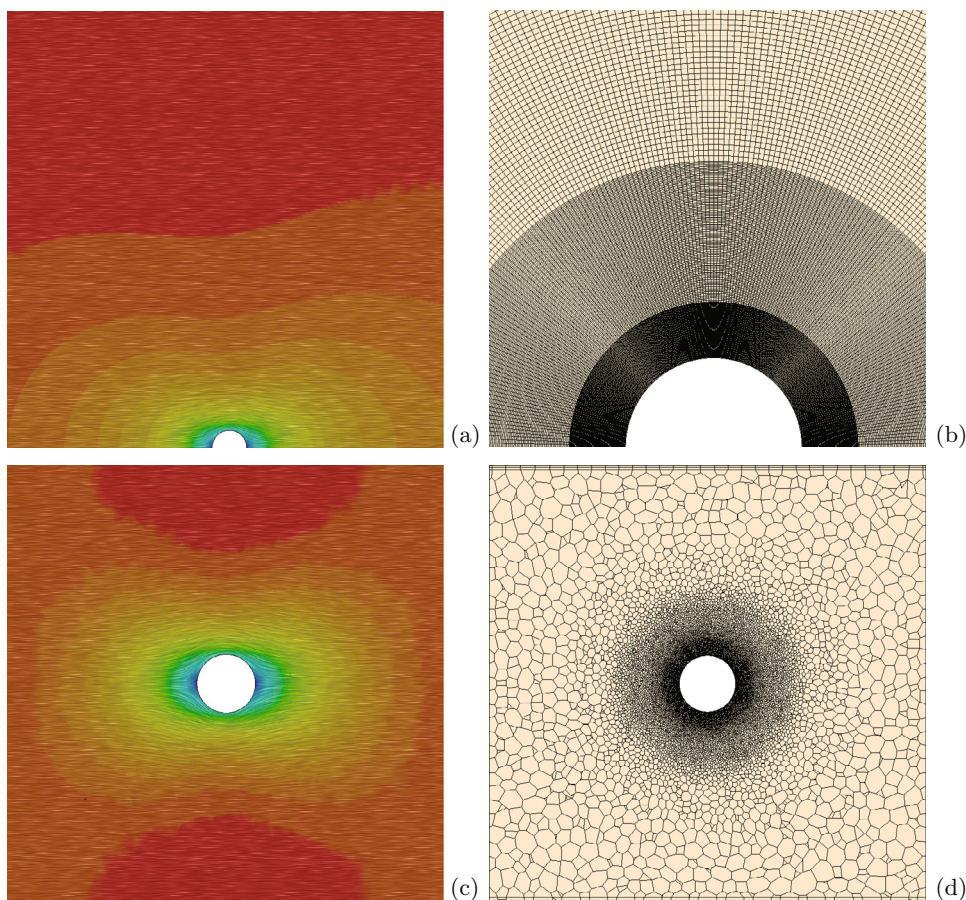


Fig. 3. Illustration of the flow past a sphere subject to Navier boundary conditions. (a) Streamlines illustrated by the Line Integral Convolution (LIC) method for the flow past a sphere in an otherwise undisturbed fluid (closeup view); (b) the corresponding mesh (closeup view); (c) streamlines (LIC) of the flow past an array of spheres; (d) the corresponding mesh. The array of spheres is realized by imposing periodic boundary conditions on side faces of the bounding box (top and bottom in (c) and (d)). The direction of the flow is from the left to the right.

simulations: simulations past a single fullerene molecule and simulations past an array of fullerene molecules.

In the first set of simulations we simulate water flow past the fullerene molecule in an otherwise undisturbed fluid flow (Fig. 3a). We place a sphere of radius $R^* = 1.00$ in the center of a spherical domain out of which we cut a 10° wedge in the azimuthal direction. This domain contains four concentric submeshes with the density of the mesh decreasing with the distance from the sphere. The density in the azimuthal and polar directions is constant through all the submeshes with 180 cells in the azimuthal direction and 2 cells in the polar direction in each submesh. In the radial direction we vary the cell density. The first subdomain extends from $r^* = 1$ to $r^* = 1.94$ with 100 cells, the second from $r^* = 1.94$ to $r^* = 3.88$ with 100 cells, the third from $r^* = 3.88$ to $r^* = 19.42$ with 200 cells and the fourth from $r^* = 19.42$ to $r^* = 194.17$ with 200 cells (Fig. 3b). This amounts to 21600 cells in total. The constant free-stream

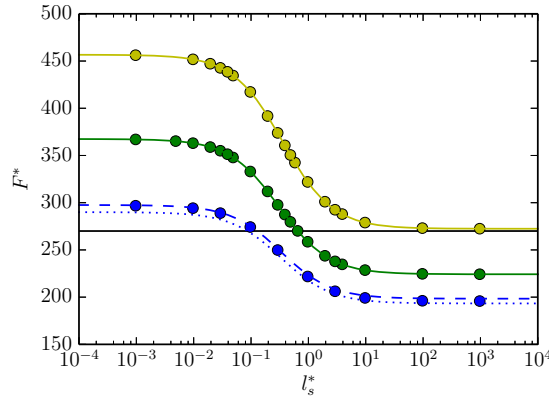


Fig. 4. Drag force dependence on the slip length. The circles represent the data points of the continuum simulations. The results in *blue* represent the drag force for a single fullerene molecule with $R_H^* = 1.00$ placed in an otherwise undisturbed fluid flow. The blue dotted and the dashed lines represent the drag force from an analytical solution in Eq. (12) and the Oseen-like correction to the analytical solution in Eq. (13) respectively. Results shown in green and yellow represent the drag force on a fullerene molecule with $R_H^* = 1.00$ and $R_H^* = 1.18$ respectively in an array of fullerene molecules forming a square lattice. The green and yellow solid lines are fits of the three parametric function in Eq. (14) to the CFD data points. The black horizontal line at $F^* = 270$ marks the drag force measured in the multiscale simulation [5].

velocity v_∞ imposed at $r^* = 194.17$, and the density ρ and viscosity μ are set to match the Reynolds number of the multiscale simulation $\text{Re} = \rho v_\infty R / \mu = 0.067$.

In the second set of simulations we set up our computational system to mimic the one from the multiscale simulation (Fig. 3c). We place the sphere in the center of a cubic box of edge $L^* = 15.53$. The coordinate axes are oriented parallel to the box edges, where the x axis points in the direction of the fluid flow. We again vary the mesh density with the distance from the sphere with the total number of cells cca. 1.7 million (Fig. 3d). At the inlet and outlet faces of the bounding box we impose a uniform fluid velocity boundary conditions and on the side faces we impose periodic boundary conditions. By using the periodic boundary conditions we simulate a flow past an array of fullerenes, which form a square lattice extending to infinity as is the case in the multiscale simulations.

Walther et al. [5] estimated the slip length and the hydrodynamic radius R_H^* (the radius at which the Navier boundary condition is imposed) by fitting the drag force and the velocity profile to the solutions for a viscous flow past a sphere in an otherwise undisturbed fluid. The drag force obtained from the multiscale simulation is $F^* = 270 \pm 15$ and the extracted hydrodynamic radius and slip length are $R_H^* = 1.18$ and $l_s^* = 0.58$. By applying this hydrodynamic radius and slip length in a CFD simulation the obtained force is $F^* = 342$, which is in reasonable agreement with the force measured in the multiscale simulation with a deviation of 25%. The 25% deviation in force is due to how the slip length and the hydrodynamic radius are obtained from the multiscale simulations. There, an analytic expression for the drag force on a single sphere in an otherwise undisturbed flow is used while the flow simulated is a flow past an array of fullerene molecules. Figure 4 shows the drag force dependence on the slip length for the fluid flow past a sphere in an otherwise undisturbed flow with $R_H^* = 1.00$ and a flow past a 2D lattice of fullerene molecules with $R_H^* = 1.00$ and $R_H^* = 1.18$. The results show that the presence of the surrounding fullerene molecules increases the drag. An analytical solution of the drag force for a

flow past a single fullerene molecule is also shown in the figure [33]

$$F^* = \frac{6\pi}{\text{Re}} \frac{1 + 2l_s^*}{1 + 3l_s^*} \quad (12)$$

and an Oseen-like correction [34]

$$F^* = \pi \left(\frac{6}{\text{Re}} + \frac{3}{1 + \sqrt{2\text{Re}}} + 0.2 \right) \frac{1 + 2l_s^*}{1 + 3l_s^*}. \quad (13)$$

In the no-slip limit Eq. (12) gives $F^* = 6\pi/\text{Re} = 290$, which results in the Stokes' law. The Oseen correction sets the drag force to $F^* = 298$, which is in excellent agreement to the drag force $F^* = 297$ from the continuum simulation. In the opposite limit to the no-slip boundary condition, where the interface friction coefficient vanishes and the slip length diverges, the perfect-slip boundary condition, Eq. (12) gives $F^* = 4\pi/\text{Re} = 193$ and the Oseen-like correction gives $F^* = 198$. The drag force measured in the CFD simulation is $F^* = 196$. The Oseen-like correction improves the prediction of the drag force in the low slip regime. In the high slip regime, however, it slightly overpredicts the drag coefficient.

Next we extract the slip length from the CFD simulations that match the drag force predicted by the multiscale simulations. We maintain a constant hydrodynamic radius of $R_H^* = 1.00$. In the Fig. 4 we fit a three parametric function

$$f(x) = a \frac{b + x}{c + x} \quad (14)$$

to the CFD data points. The three parameters in the fitting function determine the minimum, the maximum and the point of transition, and in the case of Eq. (12) they are $a = 4\pi/\text{Re}$, $b = 1/2$ and $c = 1/3$. The obtained parameters for the flow past the array of fullerene molecules are $a\text{Re}/(4\pi) = 1.1955$, $2b = 1.0062$, and $3c = 0.9213$. Using these parameters we find $l_s^* = 0.65$ by solving the inverse function of Eq. (14), $f^{-1}(x) = (ab - cx)/(x - a)$, for $x = F^* = 270$. Using $l_s^* = 0.65$ in a CFD simulation indeed results in a drag force conforming to the multiscale simulation. The parameter a gives the minimal drag force, which is reached at the perfect-slip boundary condition ($l_s^* \rightarrow \infty$). We also compare the fluid velocity profile around the fullerene molecule from the slip corrected, continuum simulations and multiscale simulation to confirm the accuracy of the continuum hydrodynamics approach. Figure 5 shows the x component of the fluid velocity along the x axis and y axis for several CFD simulations and the multiscale simulation. We observe that using $R_H^* = 1.00$ and $l_s^* = 0.65$ or $R_H^* = 1.18$ and $l_s^* \rightarrow \infty$ gives a velocity profile and drag force in better agreement to the multiscale simulation than $R_H^* = 1.18$ and $l_s^* = 0.58$. We also observe that by increasing the hydrodynamic radius and the slip length simultaneously gives similar results. With a greater hydrodynamic radius the extrapolated velocity vanishes deeper into the wall and a greater slip length is needed.

Figure 6 shows the energy dissipation rate per unit volume due to viscosity [23]

$$\dot{e}^* = \frac{1}{2\text{Re}} \left(\frac{\partial v_i^*}{\partial x_k^*} + \frac{\partial v_k^*}{\partial x_i^*} \right)^2. \quad (15)$$

The figure shows that the viscous part of the stress tensor is nonzero in the vicinity of the sphere. Thus, the viscous term in the momentum flux is also nonzero [3]

$$J_{ik}^* = v_i^* v_k^* + p^* \delta_{ik} - \frac{1}{\text{Re}} \left(\frac{\partial v_i^*}{\partial x_k^*} + \frac{\partial v_k^*}{\partial x_i^*} \right). \quad (16)$$

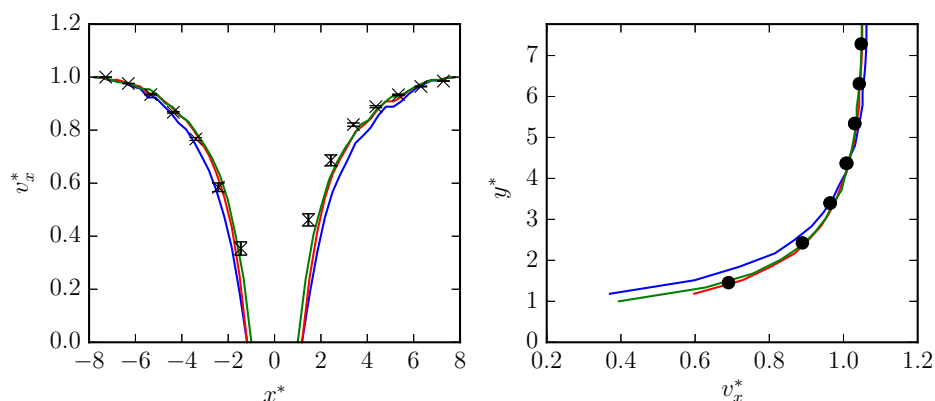


Fig. 5. Velocity profile of fluid flow around the fullerene molecule. x component of the fluid velocity along the x axis (left) and y axis (right). The black X symbols and black circles with errorbars represent the results from the multiscale simulation and the solid lines the CFD results. Green line represents results for $R_H^* = 1.00$ and $l_s^* = 0.65$, red for $R_H^* = 1.18$ and $l_s^* \rightarrow \infty$, and blue for $R_H^* = 1.18$ and $l_s^* = 0.58$.

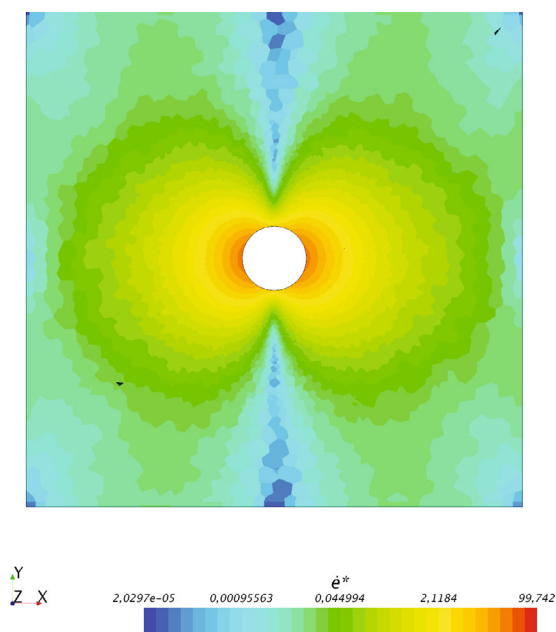


Fig. 6. Energy dissipation rate per unit volume due to viscosity for the flow past an array of spheres.

This highlights the importance of matching two adjacent grid layers at the atomistic-continuum interface as performed in the multiscale simulation [5]. This ensured the matching of the velocity gradients in addition to velocity at the interface. Without this the momentum flux would not be conserved due to the presence of the velocity gradients in the viscous term. This was not an issue in previous multiscale simulations of fluid flow past and through nanotubes [35,36]. There the atomistic-continuum interface was further away from the nanotube where the viscous part of the stress tensor is not significant and thus matching the velocity in a single grid layer did not present a problem.

4 Summary and conclusions

In summary, we have shown that the slip corrected, continuum hydrodynamics accurately describe the fluid flow past a single and an array of fullerene molecules. The effective simulation of water flows past fullerenes hinges on the appropriate description of the physical mechanisms at the interface of water with the fullerene molecule. The standard no-slip boundary conditions breaks down and a more appropriate boundary condition is needed. These boundary conditions can be obtained through atomistic simulations which can then provide suitable boundary conditions for the continuum solvers. Here we demonstrate that the simple Navier boundary condition with a linear dependence of shear stress on the slip velocity can be very effective in this task. This results suggest that we can simulate such systems using continuum simulations thus accessing spatiotemporal scales that will be inaccessible for MD simulations. Such slip corrected continuum simulations can then be a very important design tool for engineering flows that involve nanoparticles.

Open issues related to the present modeling approach include the sensitivity of the results on the slip length and the variation of the slip length on the surface properties such as curvature [7, 30, 37, 38], corrugation [39], and flexibility [40]. In addition, the uncertainty of the slip length extracted from atomistic simulations is significant [13, 28] which may limit the accuracy of the present model. Uncertainty quantification is expected to play a key role in identifying and reducing these uncertainties [41].

The authors thank CD-adapco for the support at implementing the partial-slip boundary conditions into the STAR-CD simulation package. A. P. and M. P. acknowledge financial support through grants P1-0002, J1-4134, and BI-DK/11-12-002 from the Slovenian Research Agency.

References

1. Suddhashil Chattopadhyay, Xiao-Lun Wu, *Biophys J.* **96**, 2023 (2009)
2. Matej Praprotnik, Luigi Delle Site, Kurt Kremer, *Annu. Rev. Phys. Chem.* **59**, 545 (2008)
3. Rafael Delgado-Buscalioni, Kurt Kremer, Matej Praprotnik, *J. Chem. Phys.* **128**, 114110 (2008)
4. Rafael Delgado-Buscalioni, Kurt Kremer, Matej Praprotnik, *J. Chem. Phys.* **131**, 244107 (2009)
5. Jens H. Walther, Matej Praprotnik, Evangelos M. Kotsalis, Petros Koumoutsakos, *J. Comput. Phys.* **231**, 2677 (2012)
6. Tai-De Li, Jianping Gao, Robert Szoszkiewicz, Uzi Landmand, Elisa Riedo, *Phys. Rev. B* **75**, 115415 (2007)
7. John A. Thomas, Alan J.H. McGaughey, *Nano Lett.* **8**, 2788 (2008)
8. John A. Thomas, Alan J.H. McGaughey, *Phys. Rev. Lett.* **102**, 184502 (2009)
9. Lydric Bocquet, Elisabeth Charlaix, *Chem. Soc. Rev.* **39**, 1073 (2010)
10. David M. Holland, Duncan A. Lockerby, Matthew K. Borg, William D. Nicholls, Jason M. Reese, *Molecular dynamics pre-simulations for nanoscale computational fluid dynamics. *Microfluid Nanofluid** (2014), doi: 10.1007/s10404-014-1443-6
11. Meisam Pourali, Simone Meloni, Francesco Magaletti, Ali Maghari, Carlo M. Casciola, Giovanni Ciccotti, *J. Chem. Phys.* **141**, 154107 (2014)
12. Aleksandar Popadić, Jens H. Walther, Petros Koumoutsakos, Matej Praprotnik, *New J. Phys.* **16**, 082001 (2014)
13. J.S. Hansen, Jeppe C. Dyre, Peter J. Daivis, B.D. Todd, Henrik Bruus, *Phys. Rev. E*, **84**, 036311 (2011)
14. Peter A. Thompson, Mark O. Robbins, *Phys. Rev. A* **41**, 6830 (1990)

15. V.P. Sokhan, D. Nicholson, N. Quirke, *J. Chem. Phys.* **115**, 3878 (2001)
16. Mainak Majumder, Nitin Chopra, Rodney Andrews, Bruce J. Hinds, *Nature* **438**, 44 (2005)
17. Sony Joseph, N.R. Aluru, *Nano Lett.* **8**, 452 (2008)
18. Umberto Ulmanella, Chih-Ming Ho, *Phys. Fluids* **20**, 101512 (2008)
19. K.M. Mohamed, A.A. Mohamad, *Microfluid Nanofluid* **8**, 283 (2010)
20. Mainak Majumder, Nitin Chopra, Bruce J. Hinds, *ACS Nano* **5**, 3867 (2011)
21. Lydric Bocquet, Jean-Louis Barrat, *Soft Matter* **3**, 685 (2007)
22. G.H. Atefi, H. Niazmand, M.R. Meigounpoory, *J. Disp. Sci. Tech.* **28**, 591 (2007)
23. L.D. Landau, E.M. Lifshitz, *Fluid Mechanics*, Vol. 6, *Course of Theoretical Physics*, 2nd edition (Butterworth-Heinemann, 1987)
24. Dietrich Einzel, Peter Panzer, Mario Liu, *Phys. Rev. Lett.* **64**, 2269 (1990)
25. Kerstin Falk, Felix Sedlmeier, Laurent Joly, Roland R. Netz, Lydric Bocquet, *Nano. Lett.* **10**, 4067 (2010)
26. Kerstin Falk, Felix Sedlmeier, Laurent Joly, Roland R. Netz, Lydric Bocquet, *Langmuir* **28**, 14261 (2012)
27. J.S. Hansen, B.D. Todd, Peter J. Davis, *Phys. Rev. E* **84**, 016313 (2011)
28. Sridhar Kumar Kannam, B.D. Todd, J.S. Hansen, Peter J. Davis, *J. Chem. Phys.* **135**, 144701 (2011)
29. Sridhar Kumar Kannam, B.D. Todd, J.S. Hansen, Peter J. Davis, *J. Chem. Phys.* **136**, 244704 (2012)
30. Sridhar Kumar Kannam, B.D. Todd, J.S. Hansen, Peter J. Davis, *J. Chem. Phys.* **136**, 024705 (2012)
31. Sridhar Kumar Kannam, B.D. Todd, J.S. Hansen, Peter J. Davis, *J. Chem. Phys.* **138**, 094701 (2013)
32. CD-adapco *STAR-CD version 4.18 Documentation*, 2012
33. B.S. Padmavathi, T. Amaranath, S.D. Nigam, *Fluid Dyn. Res.* **11**, 229 (1993)
34. Frank M. White, *Viscous Fluid Flow*, 2 edition (McGraw-Hill, 1991)
35. A. Dupuis, E.M. Kotsalis, P. Koumoutsakos, *Phys. Rev. E* **75**, 046704 (2007)
36. Thomas Werder, Jens H. Walther, Petros Koumoutsakos, *J. Comput. Phys.* **205**, 373 (2005)
37. J.H. Walther, T. Werder, R.L. Jaffe, P. Koumoutsakos, *Phys. Rev. E* **69**, 062201 (2004)
38. Weikang Chen, Rui Zhang, Joel Koplik, *Phys. Rev. E* **89**, 023005 (2014)
39. S. Richardson, *J. Fluid Mech.* **59**, 707 (1973)
40. Vladimir P. Sokhan, David Nicholson, Nicholas Quirke, *J. Chem. Phys.* **117**, 8531 (2002)
41. P. Angelikopoulos, C. Papadimitriou, P. Koumoutsakos, *J. Phys. Chem. B* **117**, 14808 (2013)